<Electronic Supplementary Information>

Structural properties of [$Cu(II)_3L_6$] cages: bridged polyatomic anion effects on unprecedented efficiency of heterogeneous catechol oxidation

Doheon Kim, Geonwoo Gwak, Jihun Han, Dongwon Kim, and Ok-Sang Jung*

Department of Chemistry, Pusan National University, Busan 46241, Republic of Korea Fax: (+82) 51-5163522;

Tel: (+82) 51-5103240; E-mail: oksjung@pusan.ac.kr

Table S1 Selected bond lengths and angles

$SiF_6@[Cu_3L_6](\mu_2\text{-}SiF_6)_{1.5}(BF_4)\cdot 6MeOH$		$SiF_6@[Cu_3L_6](\mu_2\text{-}SiF_6)_{1.5}(ClO_4)\cdot 6MeOH$		$SiF_6@[Cu_3L_6](SbF_6)_4$		$PF_6@[Cu_3L_6(MeOH)_3](PF_6)_5\cdot 2MeOH$	
Cu(1)-N(1)	1.989(9)	Cu(1)-N(2A)	1.989(5)	Cu(1)-N(13)	1.973(11)	Cu(1)-N(1F)	2.009(5)
Cu(1)-N(3)	1.997(9)	Cu(1)-N(1B)	2.012(5)	Cu(1)-N(10)	1.992(12)	Cu(1)-N(2C)	2.023(5)
Cu(1)-N(4)$^{\#1}$	2.020(10)	Cu(1)-N(1A)$^{\#1}$	2.021(5)	Cu(1)-N(12)	1.997(10)	Cu(1)-N(2A)	2.041(4)
Cu(1)-N(2)$^{\#2}$	2.026(10)	Cu(1)-N(2B)$^{\#2}$	2.023(5)	Cu(1)-N(11)	2.017(11)	Cu(1)-N(2D)	2.045(5)
Cu(1)-F(3J)	2.35(4)	Cu(1)-F(5)$^{\#3}$	2.393(5)	Cu(1)-F(12)	2.368(12)	Cu(1)-O(2)	2.293(5)
Cu(1)-F(4I)	2.37(5)						
		N(2A)-Cu(1)-N(1B)	177.6(3)	N(13)-Cu(1)-N(10)	170.6(6)	N(1F)-Cu(1)-N(2C)	178.5(2)
N(1)-Cu(1)-N(3)	178.5(4)	N(2A)-Cu(1)-N(1A)$^{\#1}$	88.2(3)	N(13)-Cu(1)-N(12)	90.1(6)	N(1F)-Cu(1)-N(2A)	90.10(17)
N(1)-Cu(1)-N(4)$^{\#1}$	90.4(4)	N(1B)-Cu(1)-N(1A)$^{\#1}$	91.1(3)	N(10)-Cu(1)-N(12)	89.0(6)	N(2C)-Cu(1)-N(2A)	89.68(17)
N(3)-Cu(1)-N(2)$^{\#2}$	91.2(4)	N(2A)-Cu(1)-N(2B)$^{\#2}$	91.9(3)	N(13)-Cu(1)-N(11)	88.2(6)	N(1F)-Cu(1)-N(2D)	88.95(18)
N(4)$^{\#1}$-Cu(1)-N(2)$^{\#2}$	174.0(4)	N(1B)-Cu(1)-N(2B)$^{\#2}$	89.1(3)	N(10)-Cu(1)-N(11)	93.1(6)	N(2C)-Cu(1)-N(2D)	90.89(19)
N(4)$^{\#1}$-Cu(1)-F(3J)	85.4(11)	N(1A)$^{\#1}$-Cu(1)-N(2B)$^{\#2}$	173.0(2)	N(12)-Cu(1)-N(11)	176.8(6)	N(2A)-Cu(1)-N(2D)	165.93(19)
N(2)$^{\#2}$-Cu(1)-F(3J)	88.6(11)	N(2A)-Cu(1)-F(5)$^{\#3}$	90.4(3)	N(13)-Cu(1)-F(12)	96.2(5)	N(1F)-Cu(1)-O(2)	90.59(19)
N(1)-Cu(1)-F(4I)	95.0(11)	N(1B)-Cu(1)-F(5)$^{\#3}$	91.9(3)	N(10)-Cu(1)-F(12)	93.2(6)	N(2C)-Cu(1)-O(2)	90.92(19)
N(3)-Cu(1)-F(4I)	86.5(11)	N(1A)$^{\#1}$-Cu(1)-F(5)$^{\#3}$	86.2(2)	N(12)-Cu(1)-F(12)	94.8(5)	N(2A)-Cu(1)-O(2)	94.11(18)
N(4)$^{\#1}$-Cu(1)-F(4I)	88.9(15)	N(2B)$^{\#2}$-Cu(1)-F(5)$^{\#3}$	86.9(2)	N(11)-Cu(1)-F(12)	82.7(6)	N(2D)-Cu(1)-O(2)	99.93(19)
N(2)$^{\#2}$-Cu(1)-F(4I)	85.1(15)						

$^{\#1}$ y, -z+1, -x+1

$^{\#2}$ -z+1, x, -y+1

$^{\#1}$ z, -x+1, -y+1

$^{\#2}$ -y+1, -z+1, x

$^{\#3}$ -x+1, -y, z

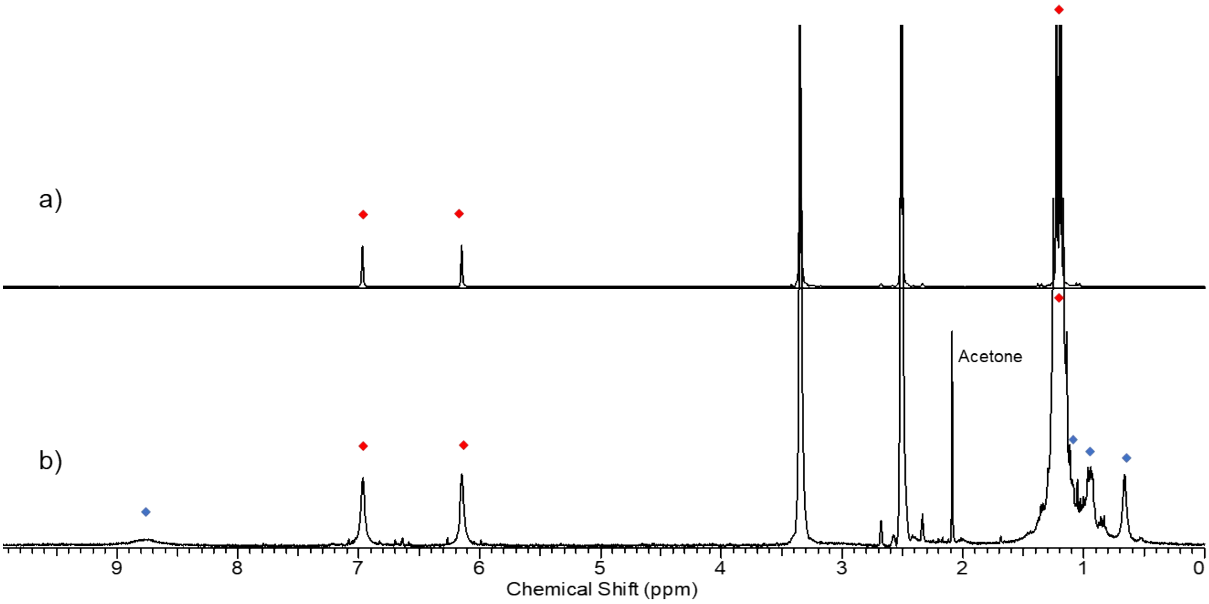

Fig. S1. [1]H NMR spectrum of authentic 3,5-di-*tert*-butylorthoquinone (a) in Me_2SO-d_6. [1]H NMR spectrum in Me_2SO-d_6 after catalysis using $SiF_6@[Cu_3L_6](\mu_2\text{-}SiF_6)_{1.5}(ClO_4)\cdot 6MeOH$ in acetone.

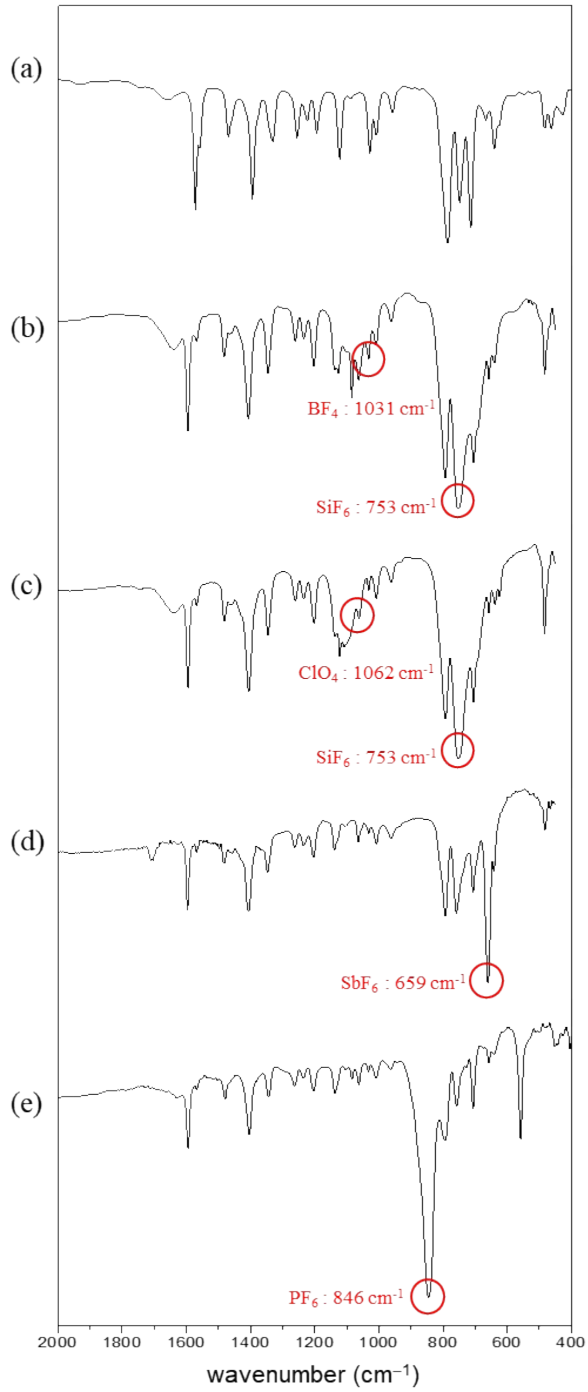

Fig. S2. FT-IR spectra of L (a), $SiF_6@[Cu_3L_6](\mu_2\text{-}SiF_6)_{1.5}(BF_4)\cdot 6MeOH$ (b), $SiF_6@[Cu_3L_6](\mu_2\text{-}SiF_6)_{1.5}(ClO_4)\cdot 6MeOH$ (c), $[Cu_3(SiF_6)L_6](SbF_6)_4$ (d), and $PF_6@[Cu_3L_6(MeOH)_3](PF_6)_5\cdot(MeOH)_2$ (e).

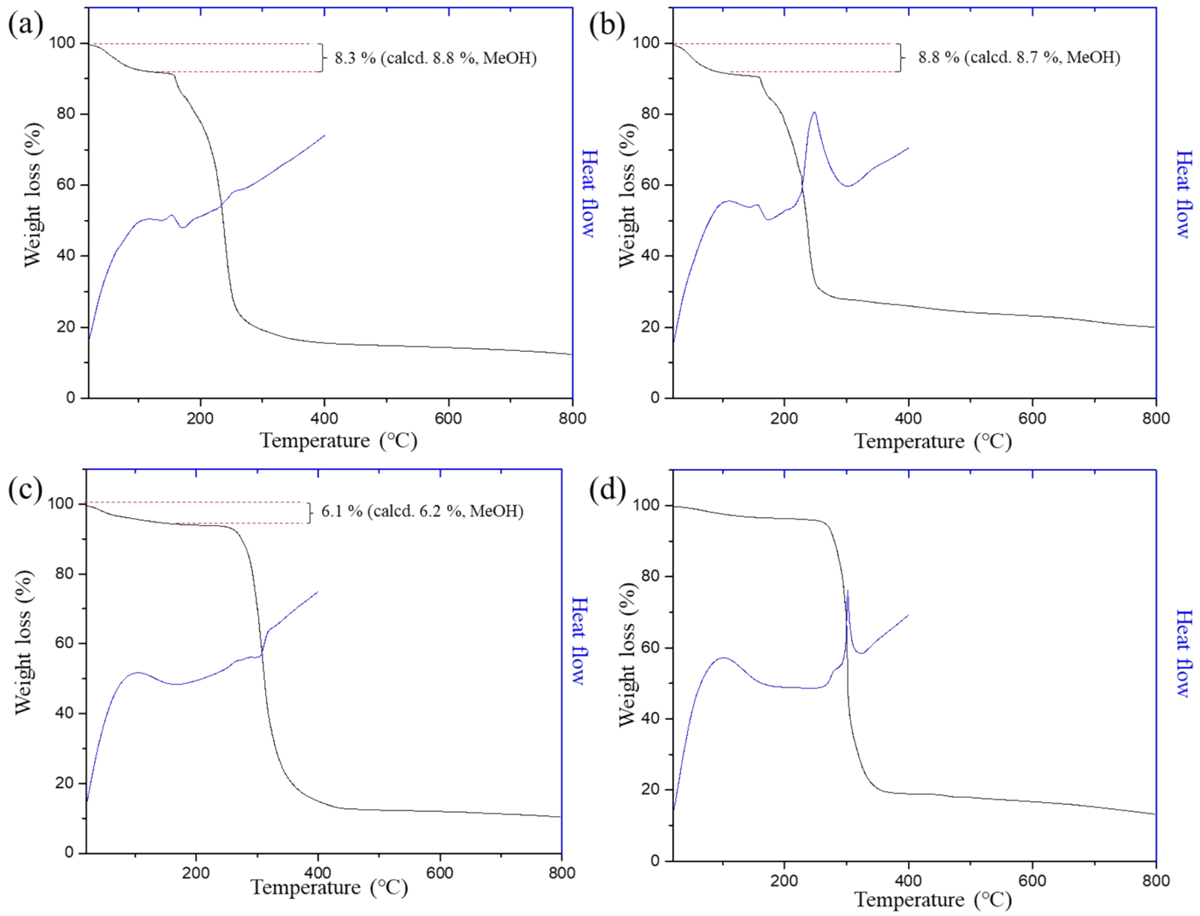

Fig. S3. TGA and DSC curves for SiF_6@$[Cu_3L_6](\mu_2\text{-}SiF_6)_{1.5}(BF_4)\cdot 6MeOH$ (a), SiF_6@$[Cu_3L_6](\mu_2\text{-}SiF_6)_{1.5}(ClO_4)\cdot 6MeOH$ (b), PF_6@$[Cu_3L_6(MeOH)_3](PF_6)_5\cdot(MeOH)_2$ (c), and $[Cu_3(SiF_6)L_6](SbF_6)_4$ (d).

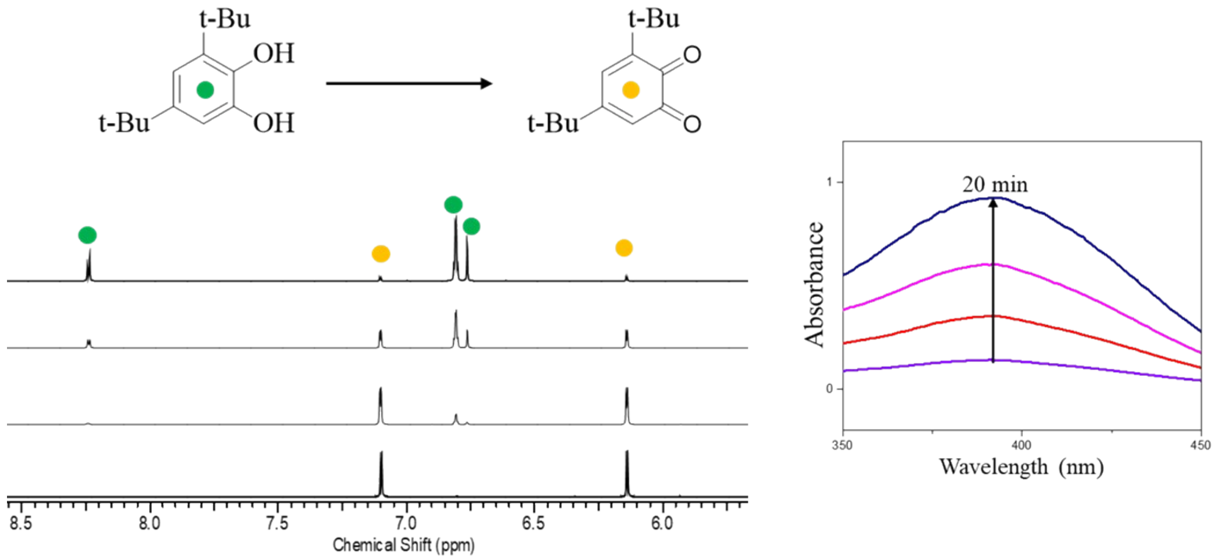

Fig. S4. [1]H NMR spectral procedure on catalytic oxidation 3,5-di-*tert*-butylcatechol to 3,5-di-*tert*-butylorthoquinone using $SiF_6@[Cu_3L_6](\mu_2\text{-}SiF_6)_{1.5}(ClO_4)\cdot 6MeOH$ in $Me_2CO\text{-}d_6$ (left). UV spectral change during the catalytic reaction (right).

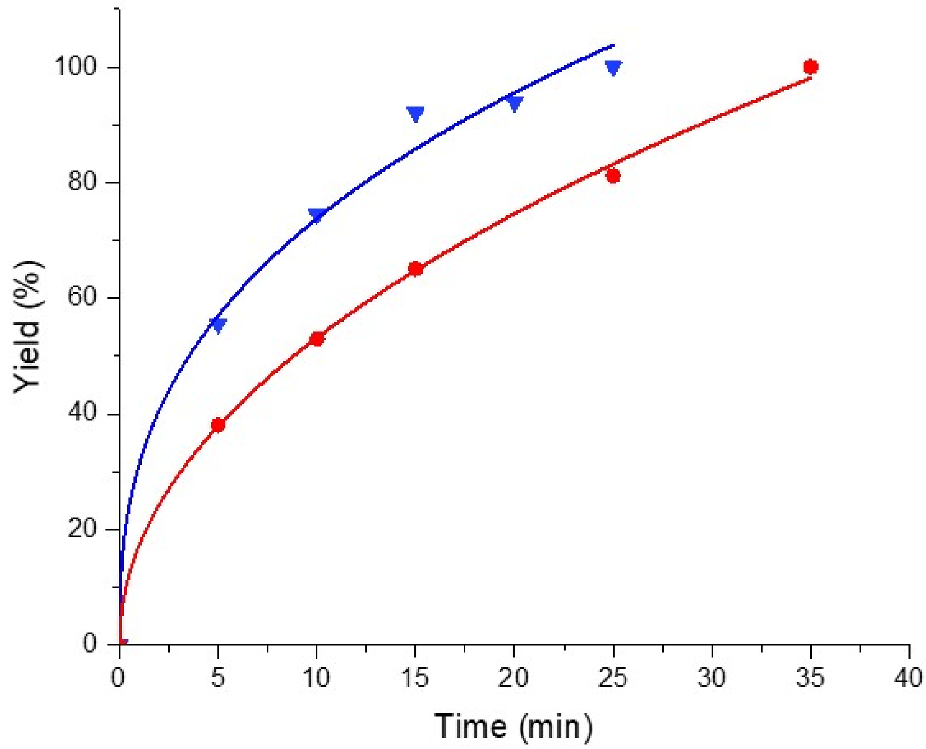

Fig. S5. Catalytic oxidation results of 3,5-di-*tert*-butylcatechol using SiF_6@[Cu_3L_6](μ_2-SiF_6)$_{1.5}$(ClO_4) in 15 mL acetone (blue line) and in 20 mL acetone (red line).

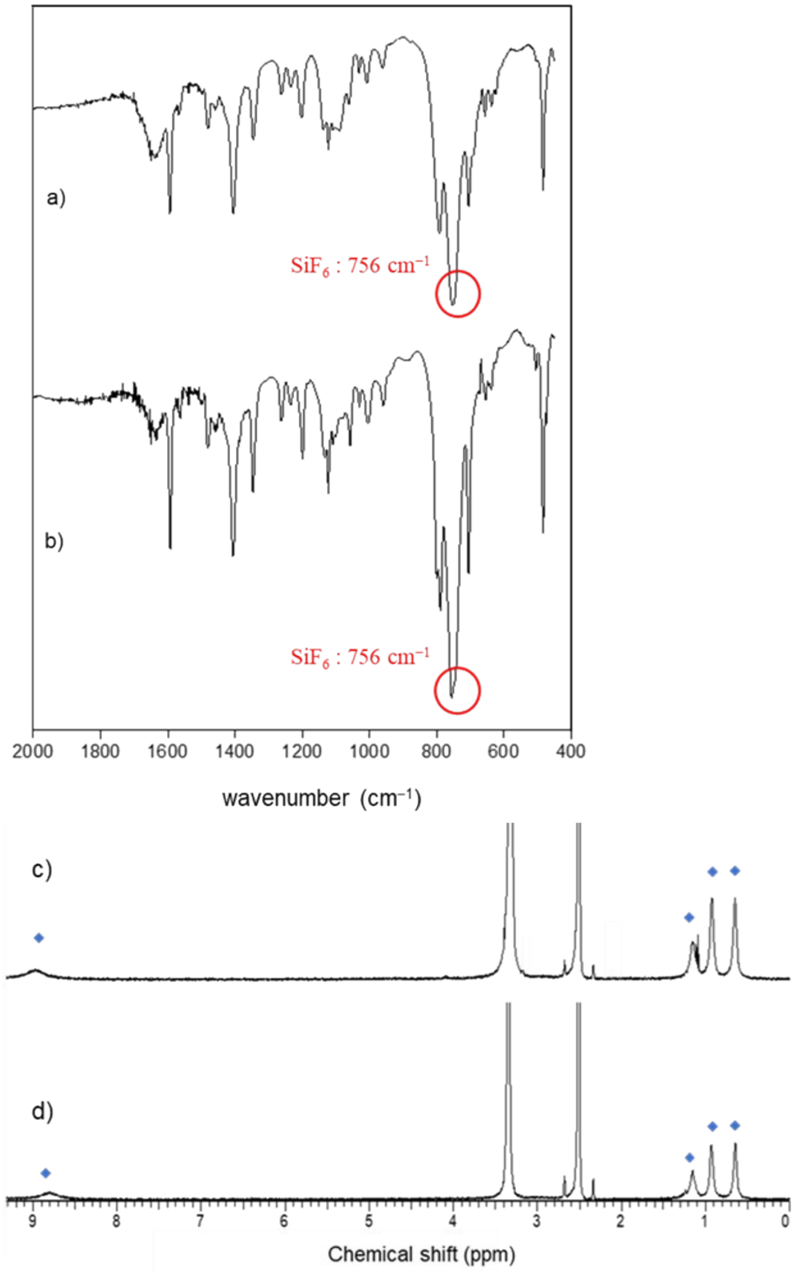

Fig. S6. IR spectra of SiF_6@$[Cu_3L_6](\mu_2\text{-}SiF_6)_{1.5}(ClO_4)\cdot6MeOH$ (a) and the recycled crystals after catechol oxidation (b). ^1H NMR spectra of SiF_6@$[Cu_3L_6](\mu_2\text{-}SiF_6)_{1.5}(ClO_4)\cdot6MeOH$ (c) and the recycled crystals after catechol oxidation (d).

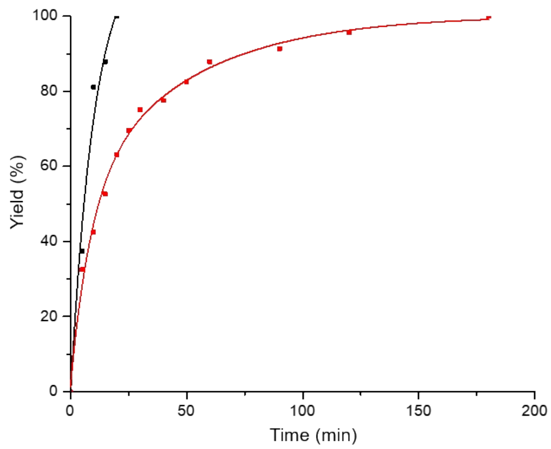

Fig. S7. Catalytic oxidation rates of 3,5-di-*tert*-butylcatechol using $SiF_6@[Cu_3L_6](\mu_2\text{-}SiF_6)_{1.5}(ClO_4)\cdot6MeOH$ (black line) and using the recycled $SiF_6@[Cu_3L_6](\mu_2\text{-}SiF_6)_{1.5}(ClO_4)\cdot6MeOH$ (red line).

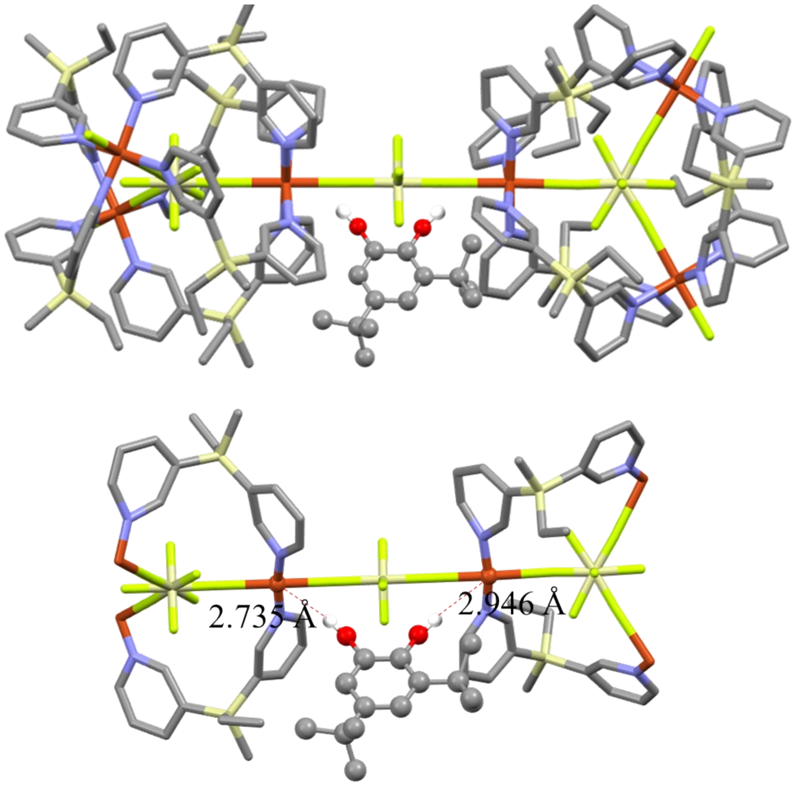

Fig. S8. Molecular model of the inter-cage Cu···Cu of heterogeneous 3D catalyst as a catalytic center and 3,5-di-*tert*-butylcatechol (OH···Cu: 2.735 – 2.946 Å).

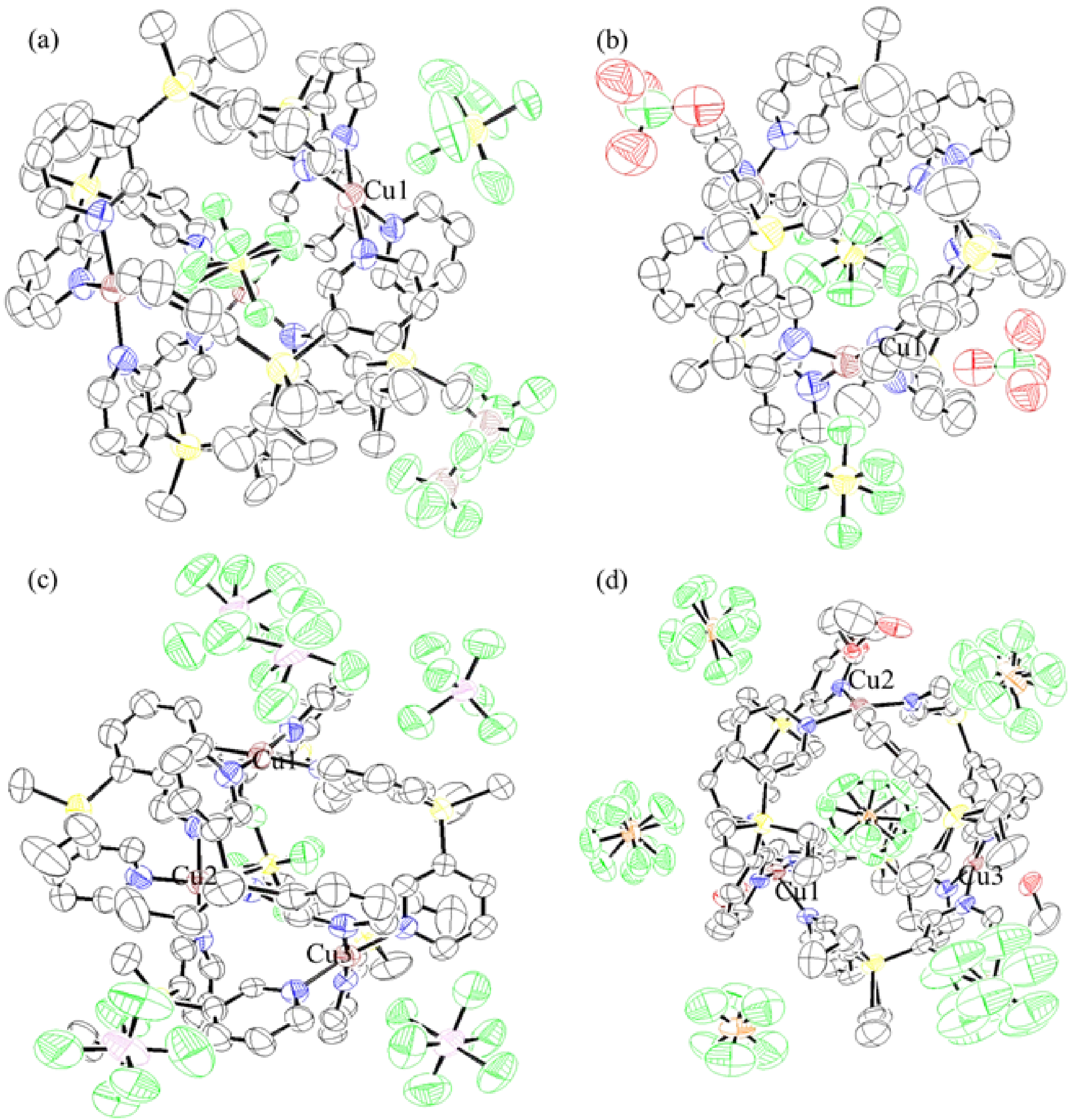

Fig. S9. ORTEP drawings of SiF_6@$[Cu_3L_6](\mu_2\text{-}SiF_6)_{1.5}(BF_4)\cdot 6MeOH$ (a), SiF_6@$[Cu_3L_6](\mu_2\text{-}SiF_6)_{1.5}(ClO_4)\cdot 6MeOH$ (b), PF_6@$[Cu_3L_6(MeOH)_3](PF_6)_5\cdot(MeOH)_2$ (c), and $[Cu_3(SiF_6)L_6](SbF_6)_4$ (d). Hydrogen atoms are omitted for clarity. Ellipsoids are depicted at 50% probability